Mid-infrared Electroluminescence in LEDs based on InAs and related alloys

A. Krier, X.L. Huang & V.V. Sherstnev*
Lancaster University,
Lancaster,
LA1 4YB, UK.
* Visiting research Fellow from The Ioffe Institute, St. Petersburg, Russia

1 Introduction

Mid-infrared light emitting diodes which operate in the (2-5μm) spectral region have been extensively studied in recent years [1,2,3] due to their increasing potential for applications in a number of areas including; optical gas sensors for pollution monitoring, remote sensing, industrial process control, spectroscopy, optical alignment and infrared countermeasures[4,5]. Consequently there has been much research interest aimed at providing monochromatic sources, such that a number of mid-infrared light-emitting diodes (LEDs) operating at different target wavelengths have now been realised[6,7,8,9]. Such sources are particularly attractive as key components in infrared gas sensor instrumentation based on optical absorption because many of the target gases, such as CH_4 CO_2 and CO, have their fundamental absorption bands in the mid-infrared spectral region. There are well established markets for infrared gas sensors, as they are recognised as being truly gas specific and therefore suitable for reliable gas detection in a wide variety of applications. Although some instruments which make use of thermal infrared sources already exist, the recent progress in developing room temperature LEDs [10,11,12,13,14] for the mid-infrared range holds considerable promise for extending the use of infrared methods still further and to provide superior instrumentation. Currently, pulsed filament sources suffer from inherently slow modulation, whereas incandescent bulbs are limited to < 4μm by the glass envelope of the source and require burning in before they become stable. From an engineering viewpoint, LEDs do not have these drawbacks and offer the additional advantages of high emittance, room-temperature operation, high modulation rate, small size, simplicity, low power consumption, and are likely to be more cost-effective than diode lasers for deployment in practical gas sensors.

In order to obtain low detection thresholds (<10ppm), the optical output power of light sources used for such applications should be as high as possible[15]. Most current sensors use low cost, simple optical arrangements which often collect only a small fraction of the radiation emitted from the source. Estimates suggest that mid-infrared LEDs must be able to produce sufficient output power (~ 10μW) within the absorption band of interest for them to be used in a practical gas sensor. The aim of this chapter is to give an overview of the physics and technology associated with the realisation of efficient mid-infrared LEDs. The physical processes which limit device performance will be considered with respect to different materials and operating conditions, to give an insight into the problems facing the design engineer.

1.1 Background

One of the first reported mid-infrared LEDs was made by Melngailis and Rediker in 1966 who produced a room temperature LED by Zn diffusion into InAs[16] and observed recombination into Zn acceptor states at 3.7μm as part of an investigation of InAs diode lasers which they were also the first to realise and report[17]. Although surprisingly effective, these devices were only homostructures and it was not long before heterojunction LEDs were fabricated using liquid phase epitaxy (LPE). The advent of epitaxial growth technology has had the effect of increasing the range of materials available which extended the wavelength range and also resulted in more efficient LEDs and lasers based on single or double heterostructures (DH). Much attention has been given to InAs and GaSb based alloys (e.g. InAsSbP, InGaAs, InGaAsSb and InAsSb) [18] as an attractive materials system for the fabrication of optoelectronic devices in the near to middle infrared wavelength region[19,20]. A number of LEDs have now been developed operating at various wavelengths covering the mid-infrared spectral region from 1-5μm. The literature is too extensive

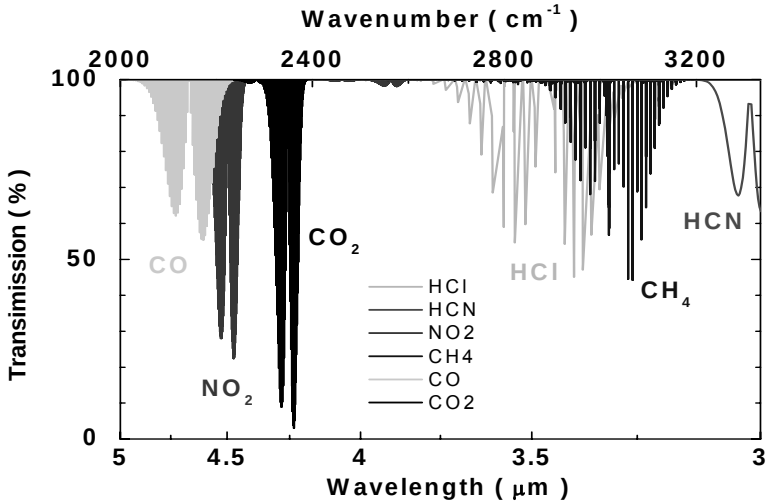

Figure 1. Some target gas absorption spectra in the mid-infrared spectral range.

to review here in detail, but recent results include, the fabrication of LEDs tuned to the absorption bands of a number of target gases, including for moisture measurement at 1.94 μm [21] , CH_4 at 3.3 μm[10] , CO_2 at 4.2 μm[22], CO at 4.6 μm[2,13] , HF at 2.5 μm[12] and the detection of H_2S at 3.8 μm[23].

With the advent of MBE and MOVPE a a variety of quantum structures have been employed to access longer wavelengths in III-V systems. These include InAs/InAsSb strained quantum well LEDs which benefit from Auger suppression in type II structures to yield emission at 5 μm and 8 μm [24, 25] which is 64% lower than the alloy band gap. Unipolar quantum cascade LEDs based on InGaAs/AlInAs

have also been able to access the 8-13 μm wavelength region but so far have only low power output (~6nW, using 20% duty cycle at 600mA) near room temperature [26,27,28]. More recently, a strained layer superlattice (SLS) LED has been demonstrated consisting of a p-i-n doped SLS grown on a mismatched InAs substrate, with a strained AlSb barrier to prevent electron migration. The LED operates at 4.2μm with an internal efficiency of 2.8%. Without the constraint of having to grow pseudomorphically on the substrate, it is envisaged that the operating wavelength may be further extended by increasing the Sb composition in the superlattice.

Room temperature electroluminescence has also been observed from InSb based sources using a thin $In_{1-x}Al_xSb$ barrier to provide carrier confinement (& exclusion)[29]. The devices have a $p^+\underline{p}^{\pm}$ л n^+ structure, with confinement of the electrons and holes in the л region provided by the wider gap $\underline{p}^{\pm}$ and degenerate n^+ regions respectively. Because of the high lattice mismatch a composition of x = 0.17 is used and the barrier thickness is kept to 20 nm consistent with strain requirements. The result is a room temperature LED which operates at 5.5 μm with an internal efficiency of 5% and an output power of 10 μW (2.5% duty cycle). The performance can be significantly enhanced by incorporation of a Winston cone into the structure to improve optical extraction [30]. Under reverse bias these $p^+\underline{p}^{\pm}$ л n^+ devices have the interesting property that they undergo minority carrier extraction at the pn junction and exclusion at the isotype junction, leading to Auger suppression[31] and negative luminescence associated with a lower than equilibrium carrier concentration in the active (л) region [32,33].

Whereas there has been a huge effort to develop HgCdTe for infrared detectors, there has been little investigation of the electroluminescence emission properties of this material [34]. However, improvements in growth by MBE and MOVPE have now led to the observation of laser action [35,36]. LPE technology has been used to grow LEDs on sapphire[37] and on CdZnTe (CZT) substrates [38] with 300K internal efficiencies as high as 6% at 3.5μm. The latter using backside emission and optical coupling with a CZT lens to increase optical extraction efficiency. More recently, similar types of $p^+\underline{p}^{\pm}$ л n^+ structures to those implemented above for InSb have been used in the HgCdTe material system resulting in emission at longer wavelengths (8-12μm) [39]. The internal quantum efficiency obtained at low injection was $4x10^{-4}$ with a maximum output power of 6nW at 295K (50% duty cycle) from an 80μm diameter LED. This low efficiency value is indicative of a large concentration of SRH centres based on a theoretical efficiency of $4x10^{-2}$ assuming an 'Auger-limited ' (CHCC) recombination mechanism.

By comparison, research on Pb-salt LEDs is very sparse indeed. Although PbSSe LEDs operating at 4.6μm with an output power of ~ 100nW at room temperature were reported some time ago[40], most research effort has been dedicated towards the fabrication of tunable diode lasers for molecular spectroscopy. The result is that Pb-salt lasers have now been developed to a high art[41,42,43], but there are surprisingly few reports concerning LEDs. Many of the problems in this material system relate to poor substrate quality and low thermal conductivity of the IV-VI material. However, the 'mirror-band' structure is less favourable for Auger recombination than in III-V's and the Auger rate in PbSe has been measured to be almost 100 times lower than that in InSb & related alloys[44]. Shi[45] has shown that

there may be some advantages in hybrid III-V/IV-VI LED and laser structures if they can be successfully grown.

2 Limitations to LED performance

2.1 Internal quantum efficiency

It is important to consider the relative importance of the different non-radiative recombination mechanisms with respect to the choice of III-V materials, the conductivity type and low or high injection conditions. Compared with GaAs LEDs which have now been developed to a very high standard, the narrow gap III-V's such as InAs have longer diffusion lengths (~25μm for electrons), lower radiative efficiency and stronger non-radiative recombination. Because the injected minority carriers are able to travel further within the material there are important consequences. Interface/surface recombination becomes more important and should be avoided, but increasing the active region width leads to increased re-absorption of the emitted light. For low injection Shockley-Read-Hall recombination (SRH) dominates but at higher injection levels Auger recombination becomes more significant. Although the injected carrier density in operational InAs-based LEDs is higher than the background doping (~10^{16}cm^{-3}), the situation is very different to that in a laser. LEDs typically operate at relatively low injected carrier densities (~10^{16}cm^{-3}) and still provide a useful total output. We conclude that SRH recombination via impurities and defects can be a significant non-radiative recombination path in InAs LEDs at room temperature under typical device operating conditions. So, it is apparent that minimising SRH recombination should be very effective in improving LED performance. Similar arguments also hold for 300K InAs detectors, and certainly for reverse-biased detectors operating in the carrier exclusion mode[46], such that reduction of SRH centres should yield performance near the theoretical limit.

The situation is rather different in InSb however, because the material contains fewer traps such that Auger recombination limits LED efficiency and is even more severe for InSb-based lasers which necessarily operate under high injection conditions. Kane et al,[47] have compared the radiative recombination efficiency of bulk p-type materials by measuring electroluminescence emission from InAs and InAsSb LEDs. Results indicate that GaAs is superior to InAs whose radiative efficiency rolls off around 3x10^{17}cm^{-3}, while $InAs_{0.9}Sb_{0.1}$ is worse still rolling off at 3x10^{16}cm^{-3}. This behaviour is consistent with the increasing importance of Auger recombination. At low injection the radiative recombination rate is proportional to np and the non-radiative recombination rate is proportional to p^2n, assuming that CHSH and CHLH Auger processes dominate in p-type material[48]. This yields for the efficiency;

$$\eta = [\ 1+ 1/B p\tau_{nr} + C_p\, p/B\ ]^{-1}, \qquad (1)$$

where τ_{nr} is the non-radiative lifetime associated with Shockley-Read processes, B is the radiative rate constant and C_p is the Auger rate constant. Experimental measurements [49,50] have produced a value of $C_p = 2x10^{-28}$ cm^6s^{-1} for low injection and indicate that original estimates for p-InAs by Takeshima[51] could easily be too large by a factor of 10. A similar consideration of efficiency in n-type III-V's reveals that Auger recombination is more severe leading to an efficiency roll off near 6×10^{15} cm^{-3} in n-InAs. This is because the CHCC mechanism is some 50 times stronger than the CHSH and CHLH processes. The result is that low p-type (л) material would be the primary choice for the LED active region at low injection. But, as injection increases the CHCC processes become progressively more significant and the efficiency decreases such that InAs LEDs with either low n or p-type active regions show similar efficiency.

As a result, there is much interest in the use of band structure engineering to produce Auger suppression in InAs alloys. The use of W- structures and strained quantum wells to modify band structure and remove holes at large k is finding successful application particularly in lasers where the injection levels are high. However, for LEDs one could argue that the minimisation of SRH recombination is more important and the approach must be to eliminate non-radiative recombination centres by removing unwanted impurities and native lattice defects. This essentially requires that one should further purify the epitaxial material in the LED active region. This has been the approach used in our laboratory to realise improved InAs and InAsSb LEDs and is described in the next sections.

2.2 Purification using rare earth gettering and Pb neutral solvent epitaxy

InAs has a room temperature energy bandgap of 0.354eV (λ_g = 3.5 μm) and so is a good choice as a starting point for the active region in the fabrication of LEDs spectrally tuned for methane detection near 3.3μm. However, although there have been a number of investigations into the electrical properties of epitaxial InAs grown from the liquid phase [52], the corresponding studies of the associated optical properties have received little attention. One approach to obtain a reduction of SRH recombination and to improve the quantum efficiency of InAs has been to use different melt purification techniques during LPE growth. These include both rare earth gettering and neutral solvent epitaxy.

The purity and quality of epitaxial InAs depends principally on the number of residual impurities and the number of structure defects. Various methods to prepare device quality InAs epitaxial layers with a low residual carrier density and a high electron mobility have been investigated. For example, purification of the starting materials (InAs and In) by prolonged annealing can reduce the impurity concentration and the corresponding residual electron density by an order of magnitude (from 10^{17} to 10^{16} cm^{-3}). The concentration of volatile impurities which result in 1-3 meV shallow donors can be further reduced by the addition of small quantities of rare earth ions. The common impurities (for example, S, Se, Si, C, Te,

O, etc.) can readily form stable compounds with reactive rare earth elements such as Gd, Yb, and Er [53]. These compounds are insoluble in indium solution and are not thought to be incorporated into the grown solid epitaxial layer and therefore rare earth gettering is an attractive means of removing unwanted impurities from LPE grown InAs solid solutions and reducing the background doping level towards 10^{15} cm^{-3}.

2.3 Purification of epitaxial InAs using Gd gettering

As mentioned earlier, room temperature quantum efficiency in narrow gap LEDs is low and is thought to be limited by band-to-band Auger recombination. However, the lower the injected carrier concentration the more likely it is that SRH recombination will be significant compared with Auger recombination and particularly if the devices are not actually operating at the Auger limit. Undoped melt grown InAs which is the basic substrate material for detectors and LEDs in the 2-5μm range is naturally n-type and usually contains residual donors of comparably high concentration (> $2x10^{16}$ cm^{-3}). Unintentionally doped InAs alloy layers grown by liquid phase epitaxy are also n-type with a background concentration of around 10^{16}-10^{17} cm^{-3}, whereas lower residual carrier concentrations (~10^{15} cm^{-3}) are obtainable using MBE or MOVPE. However, because LPE growth occurs at thermodynamic equilibrium the crystalline perfection of the resulting material is superior, making LPE material an attractive and inexpensive choice for mid-infrared optoelectronics provided the residual carrier concentration can be reduced. By adding small quantities of Dy or Gd to the melt it has been shown that the background carrier concentration in InGaAs (and InAs) can be reduced to ~ $3x10^{15}$ cm^{-3} [54,55,56,57]. This is possible because the rare earths form stable R.E. silicides/sulphides in the melt (e.g. DySi or Gd_2S_3) and these compounds are insoluble in indium which effectively reduces the incorporated shallow donor concentration in the solid layer. (Gettering of acceptors also occurs but at a lower rate because the intermetallic compounds Dy_2Zn_3 and Dy_2Mg_3 form less easily). Also it has been shown that rare earth elements themselves do not incorporate readily into the epitaxial layer at concentrations below ~0.8at% [58]. This has important consequences for LEDs (and detectors) based on these materials. Rare earth gettering can be expected to improve the quantum efficiency of InAs by; reduction of trap/recombination centres associated with impurities and reduction of background carrier concentration by removal of unintentional donors.

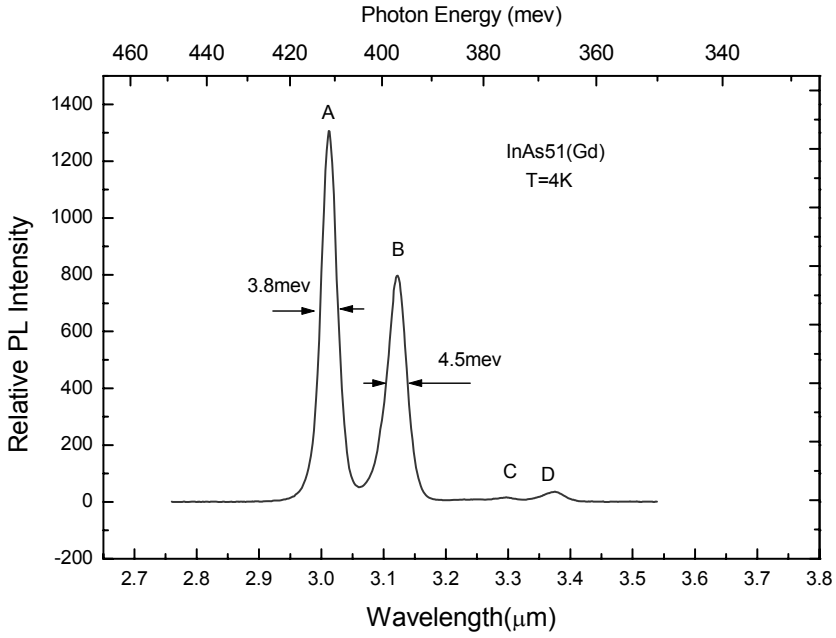

Figure 2. Low temperature photoluminescence spectrum of InAs prepared using Gd gettering of the melt during LPE growth (after Gao *et al.* [60])

High quality epitaxial InAs has been grown by LPE with the addition of small amounts of the rare earth element Gd as an impurity gettering agent added to the growth melt[59,60]. The InAs(Gd) epitaxial layers exhibited n-type conduction with Gd mole fraction lower than 3×10^{-4}, increasing above this value the epitaxial layers became p-type. When a Gd mole fraction of 1.84×10^{-5} was used then a minimum residual electron concentration of $6\times10^{15}cm^{-3}$ was obtained at liquid nitrogen temperature in good agreement with previous work[61]. The carrier mobility was measured to be $75000cm^{2}V^{-1}s^{-1}$. The photoluminescence emission intensity also increased by at least a factor of 10, due to a reduction in Shockley-Read-Hall centres.

As shown in figure 2 the purified InAs(Gd) layers exhibited 4 peaks in the 4K photoluminescence emission spectrum at (A) 411meV, (B) 397meV, (C) 376meV and (D) 367meV respectively Peaks A and B were identified as originating from bound exciton and donor-acceptor transitions respectively[62] whereas C and D were much weaker and were attributed to defects or impurity related transitions reported previously in the literature[63]. The strong increase in photoluminescence intensity

and the spectral linewidth narrowing arise due to a reduction in the residual impurity concentration (and corresponding number of non-radiative recombination centres). This is directly attributable to the gettering effects of the (Gd) rare-earth ions which were intentionally added to the melt. Compared with untreated InAs layers, the PL emission intensity of the InAs(Gd) epitaxial layers is much stronger and sharper. The linewidth (FWHM) of the bound exciton peak was measured to be 3.8meV, which is narrower than in much MBE and MOVPE grown InAs epitaxial material [64,65,66] with carrier concentration lower than $5\times10^{15}cm^{-3}$. These results confirm that both the optical and electrical properties of LPE grown InAs and its III-V alloys can be substantially improved by introducing small amounts of Gd into the growth solutions as a gettering agent and that as a direct consequence there should be corresponding significant device improvements.

2.4 Fabrication of InAsSb LEDs at 4.6μm

Melt purification techniques can be effectively extended and applied to other alloys as well as binary InAs. For example, the InAsSb ternary alloy has been purified using the rare earth ion Yb as the gettering agent and LEDs have been fabricated containing a purified ternary InAsSb active region. The 300K electroluminescence emission spectrum from one of these LEDs is shown in figure 3, where the absorption from atmospheric CO_2 at 4.2μm is clearly visible and the LED emission has a peak wavelength of 4.6μm.

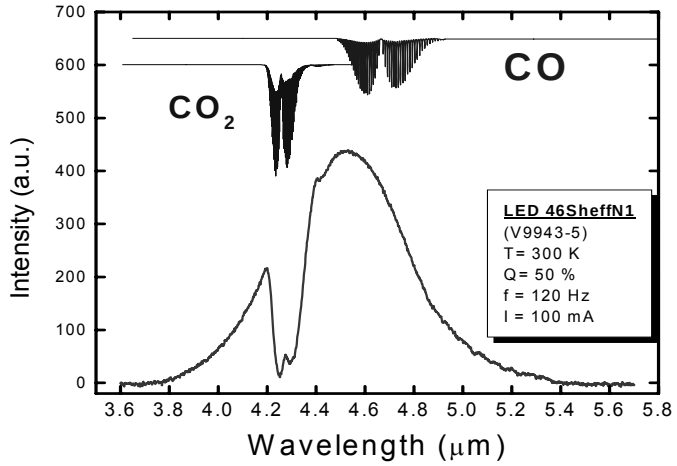

Figure 3 The electroluminescence emission spectrum of an $InAs_{0.89}Sb_{0.11}$ LED at 300 K

The LED structure, which has been described in detail previously elsewhere[67], consisted of two cladding layers of n^+ $InAs_{0.65}Sb_{0.15}P_{0.30}$ and p^+ $InAs_{0.65}Sb_{0.15}P_{0.30}$ and an undoped active region of $InAs_{0.89}Sb_{0.11}$ sandwiched between them. Because

the $InAs_{0.89}Sb_{0.11}$ ternary active region material has a large lattice mismatch with respect to the InAs substrate layer, a buffer layer with an intermediate composition ($InAs_{0.94}Sb_{0.06}$) having a 0.41% positive mismatch to the InAs substrate layer was introduced in the structure between the substrate and the n-type $InAs_{0.65}Sb_{0.15}P_{0.30}$

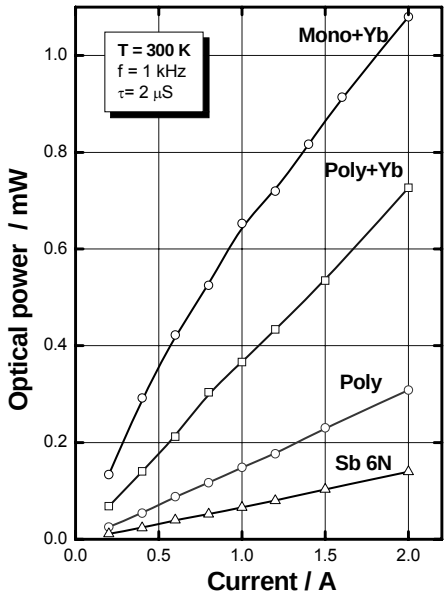

Figure 4 The optical output power characteristics measured from 4.6 μm LEDs prepared with different purification treatments of the InAsSb active region (after Krier *et al*.)

layer to reduce dislocations and to relieve strain caused by the lattice mismatch. The growth melts for the InAsSb alloy epitaxy were prepared in a similar manner to those for the growth of InAs above. However, in order to investigate the effect of material purity directly on the quantum efficiency of the active region, 4 different types of devices were fabricated in which the same epitaxial growth was used for each, but the nature of the antimony source material was different. The different precursors used in the growth melt of the active region were as follows: 6N's Sb metal, polycrystalline InSb, polycrystalline InSb +Yb and monocrystal InSb+Yb. In this experiment, we expect the improvement in precursor material purity (in going from metal to polycrystalline to monocrystal material) to result in increasingly pure epitaxial layers of InAsSb. The purpose of the Yb was to act as a gettering agent in the growth solution in order to remove S, Si impurities and to further improve the quantum efficiency of the layer. Fig. 4 shows the optical output power from each of these four types of devices. (The current used for the comparison was 2μs pulse duration at a frequency of 1kHz). From these experimental curves, it can be seen that as the purity of the precursors used in the preparation of the active region goes up, the output power exhibits a large improvement. In fact, the output power of the device grown from monocrystal InSb and Yb was 8 times larger than that grown from Sb metal at 2A drive current. This is clear evidence that improving the purity of the precursor materials used in the LPE growth melt results in a reduction of the residual carrier concentration and defects which reduce Shockley-Read-Hall recombination (SRH) in the active region. This is entirely consistent with the

improvements obtained in the PL investigation of InAs discussed above, where the photoluminescence intensity of Gd-treated InAs was improved by 10 to 100 times compared to the undoped epitaxial InAs at low temperature. The results also indicate that SRH recombination is more significant than Auger recombination in InAsSb LEDs at room temperature. At first sight this is inconsistent with other reports concerning mid-infrared lasers in the literature which are predominantly Auger limited near room temperature. However, the injected carrier concentration in an operational LED is much lower ($<10^{16}$ cm^{-3}) than in a laser ($>10^{18}$ cm^{-3}) and therefore SRH recombination (which is proportional to n and not n^3) can become the dominant non-radiative mechanism. Consequently, reducing the concentration of SRH centres using rare earth gettering can be used to major advantage in LEDs.

2.5 InAs LEDs for methane detection at 3.3μm

The rare earth gettering technique can also be applied to produce powerful InAs LEDs by following the same procedures used for InAsSb above. However there are some important differences that arise due to the type II nature of the InAs/InAsSbP heterointerface of the DH. LEDs have been fabricated in which the unintentionally doped n-InAs active layer is enclosed between p- and n- InAsSbP confinement layers. The P content in the confinement layers was 0.40 (Eg = 570 meV, T = 300 K) to provide a higher bandgap energy and large interface band offsets for good electron confinement. The InAs active region was 0.7μm thick (Eg = 354 meV, T = 300 K), and the InAsSbP layers were iso-periodic with InAs and each 3.0μm in thickness. The cladding layers were doped with Sn up to a concentration of

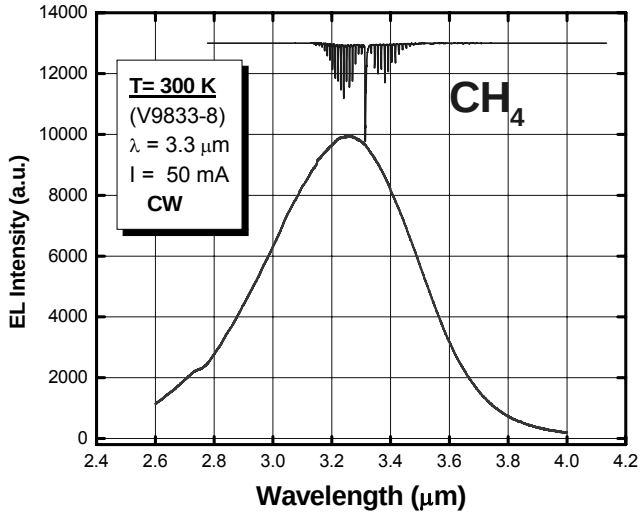

Figure 5 The electroluminescence emission spectrum of an InAs double heterostructure LED at 300 K

$5x10^{18}$ cm^{-3} and with Zn up to $1x10^{18}$ cm^{-3} for n- and p- sides respectively. By using Yb rare earth gettering the residual carrier concentration in the active layer was reduced to < $5x10^{15}$ cm^{-3}.

The quasi-continuous electroluminescence emission spectrum of one such InAs LED at room temperature is shown in figure 5. A single peak is obtained at 3.28μm which is coincident with the Q-branch absorption of methane gas. Furthermore, the LED peak wavelength remains constant over the whole range of drive currents used, unlike the situation in bulk InAs homojunction LEDs. The full width at half maximum (FWHM) of the spectrum increases only slightly with drive current and was measured to be 500 nm for these 3.28μm LEDs. The InAs/InAsSbP heterostructure is type II in nature and although the structure contains no quantum wells, the band bending at the interface leads to some confinement of electrons and holes on opposite sides, which affords the possibility of reduced Auger recombination and increased electroluminescence at room temperature. The peak wavelength of 3.28μm is not the same as that expected from the InAs energy gap, i.e λ_g = 3.50μm at 300K. The emission is also observed to be more intense than in similar epitaxial homo-junction InAs LEDs. Electroluminescence at higher energy than the bandgap (i.e. 3.28μm) and which is insensitive to drive current is consistent with emission originating from type II recombination at the InAs/InAsSbP heterojunction interface.

We can account for the improvements in output power in these LEDs by simply considering the carrier recombination mechanisms which are operating in the diode. At equilibrium, the total recombination rate, R_{tot} per unit area is given by [68]

$$R_{tot} = e\,(A_{SRH}n + B_{Rad}n^2 + C_{Auger}n^3)\,d \qquad (2)$$

where n is the carrier density in the active layer, e is the electronic charge, and d is the thickness of the active layer. The total recombination rate R_{tot} includes band-to-trap non-radiative recombination $A_{SRH}.n$, band-to-band radiative recombination $B_{Rad}.n^2$, and Auger recombination $C_{Auger}\,n^3$. The coefficient C has an exponential temperature dependence and takes the following form:

$$C_{Auger} = Co\,\exp^{-Ea/kT}, \quad \text{where} \quad E_a = [m_e/(2m_{hh})]E_g \qquad (3)$$

where E_a is the activation energy for the Auger process (and m_e and m_{hh} are the respective electron and heavy hole effective masses).
The total output power has been increased by minimising the non-radiative recombination in two ways. Firstly, because the dominant radiative transition occurs across the interface and is type II in nature, since the electrons and holes are localised on opposite sides of the heterojunction, then Auger recombination is directly suppressed and the coefficient C is reduced in the above equation. Because these levels are localised there is little wavelength shift with increasing drive current. Secondly, using Yb ions as gettering agents for the melt purification during LPE growth of the LED active region reduces the number of non-radiative

recombination centres and so directly reduces the coefficient A. Because reducing the number of such centres and shallow donors also reduces the residual carrier concentration this indirectly reduces the last term $C_{Auger}n^3$ [69]. The relative importance of the two terms $A_{SRH}.n$, and $C_{Auger}\ n^3$ depends on the temperature and also on the injection level in the device when it is operating. In this respect the $A_{SRH}.n$ term is thought to dominate at low temperatures, while $C_{Auger}\ n^3$ dominates at room temperature. This is certainly the case under high injection conditions. But, for LEDs where the injection level is lower (typically < $5x10^{16}cm^{-3}$), SRH recombination is also important, which is why an improvement due to the Yb gettering is obtained at 300K.

2.6 Neutral Solvent Epitaxy

The LPE growth of InAs from In-rich solutions has been investigated and it has been established that because epitaxy occurs below the binary melting point, As deficiency results in the formation of arsenic vacancies V_{As} in the solid, which can lead to structure defects or complex defects (V_{As}-impurity) which manifest themselves as donor or acceptor levels in the InAs band gap. There is evidence that arsenic vacancies (V_{As}) produce donor levels 43 meV below the conduction band and that complex defects result in deep acceptors [70]. Instead of using indium solution, the use of lead as a neutral solvent during growth of n-type InAs by liquid phase epitaxy makes it possible to adjust the ratio of In to As in the molten solution by varying the concentration of Pb and thus to prepare materials with reduced concentrations of structure defects. Electrical measurements on such samples have

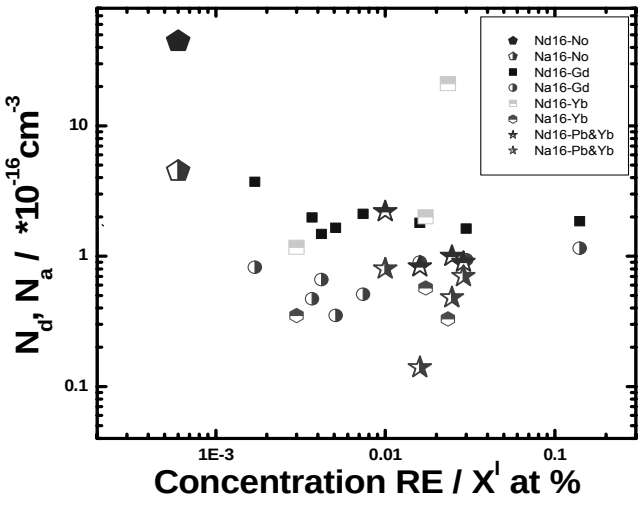

Figure 6. The dependence of residual impurity concentration on the rare earth gettering or melt purification methods used.

so far confirmed that epitaxial InAs with a low residual carrier density and a high mobility (n = $6x10^{15}$ cm^{-3} and μ_{77} ~54000 $cm^2V^{-1}s^{-1}$) can be obtained at a growth temperature of ~650 ^{0}C using lead concentration of ~63 mole% in the molten solution.

Figure 6 shows the dependence of the residual impurity concentration of the active region in response to the different melt purification techniques, based on Hall effect measurements. The results indicate that electrically the better material was obtained when Pb neutral solvent solution was used together with an additional amount of Yb. Using In solution and Yb alone produced superior results compared with Gd, which gave some improvements over the untreated samples, although the results were not entirely reproducible due in part to the small amounts of Gd or Yb being added. In order to investigate the effect of material purification on the quantum efficiency of the active region, a number of lattice-matched InAsSbP/InAs/InAsSbP double heterojunction devices were fabricated in which the same epitaxial growth procedure was used for each, except for the production of the active region. Devices with InAs active regions grown from In-rich solutions in the normal way were compared with others in which the InAs was grown using a neutral solvent - i.e. Pb as indicated above. In other experiments small quantities of either Yb or Gd were added to the In-rich growth solution for comparison with rare earth gettering effects. The mole fractions in the growth solution were typically X^l_{In} = 0.918 and X^l_{As} = 0.082 ($X^l_{R.E.}$ = 0.001 – 0.02 mol. %) respectively, corresponding to a liquidus temperature of ~610 ^{o}C. The LEDs containing InAs grown from Pb neutral solvent solution were grown using the mole fractions X^l_{Pb} = 0.664, X^l_{In} = 0.318 and X^l_{As} =

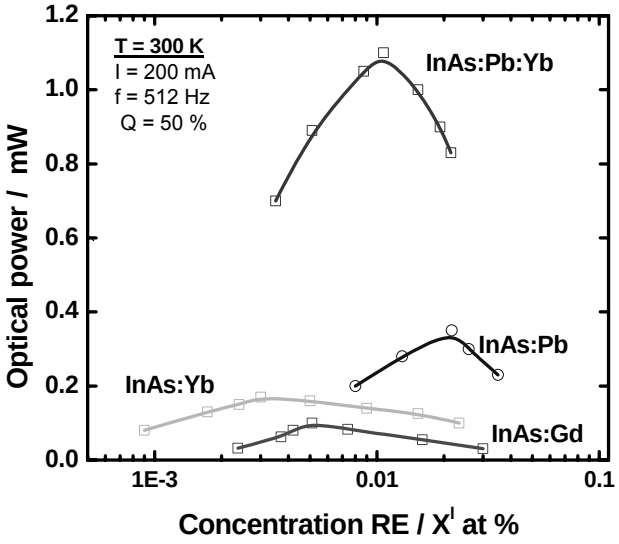

Figure 7. The dependence of the LED output power on concentration for the different purification methods used.

electron concentration in the investigation of electrical and transport properties carried out in previous work . In all cases LPE growth was carried out using the step cooled technique with a supercooling of 7^0C.

Figure 7 shows the results obtained from a comparison of the LEDs fabricated from samples with the corresponding active region treatments. A similar trend in the electroluminescence efficiency as found in the electrical results is observed, with the Pb neutral solvent solution and Yb together giving by far the best performance. We conclude that using the Pb neutral solvent solution to adjust the stoichiometry and reduce the As vacancies can be more effective than using Gd or Yb gettering to remove residual impurities. But, clearly the addition of Yb to the Pb neutral solvent gives a further improvement.

Figure 8 shows the light-current density characteristics measured from LEDs prepared with different purification treatments of the active region and using

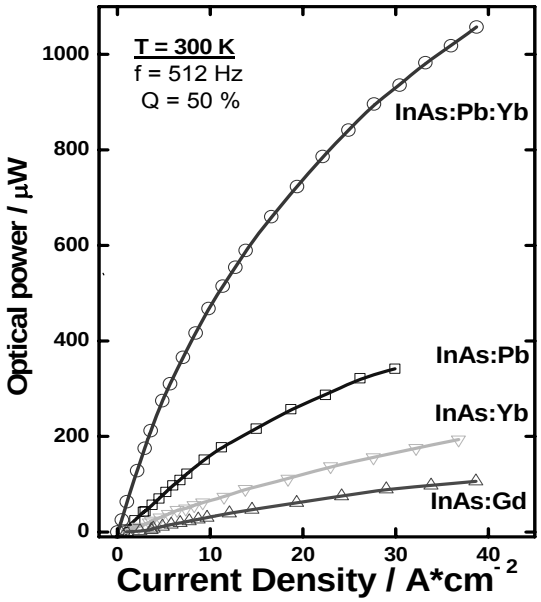

Figure 8. Light-current density characteristics measured from LEDs prepared with different purification treatments of the active region, Circles - InAs: Pb: Yb, squares - InAs: Pb, triangles down - InAs: Yb, triangles up - InAs: Gd

samples chosen from figure 7 having the optimum rare earth concentrations in each case[71]. The LEDs show excellent output with saturation occurring only at higher current densities. These results are re-plotted in figure 9 where the slope z identifies the dominant recombination mechanism. In the low current range SRH recombination dominates and the slopes are all ~1, followed by radiative recombination in the mid current region until Auger recombination begins at higher injected carrier concentrations. Clearly the InAs:Pb LED appears best throughout the entire range due to the higher purity and structural perfection of the active region.

Although Auger recombination is thought to be a limitation to the operation of room temperature mid-infrared sources these results indicate that the elimination of Shockley-Read-Hall recombination centres is important at low injection. Auger recombination is a three carrier process and the overall rate depends on n as ~ Cn^3

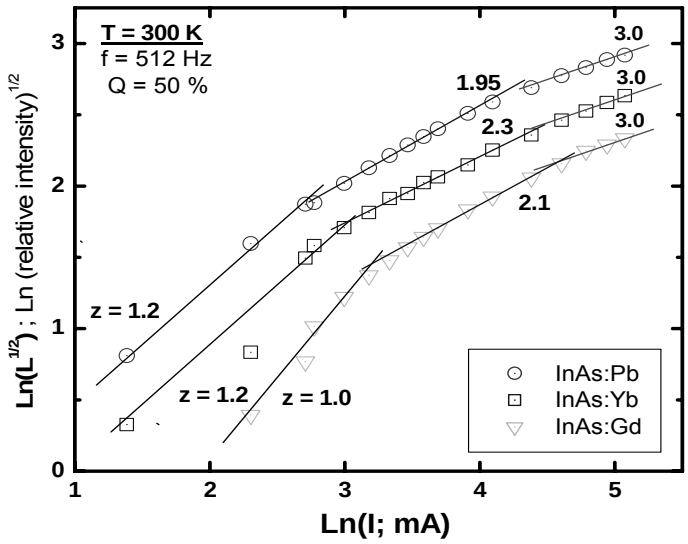

Figure 9. The relative electroluminescence intensity (L) – current (I) characteristics measured from the various LEDs plotted as ln ($L^{1/2}$) against ln (I): circles – InAs: Pb, squares - InAs: Yb, triangles - InAs: Gd. The slope represents the index z in the equation $I = An+Bn^2+Cn^3$ and reveals the different recombination mechanisms operating as the current injection increases .

where C is the Auger coefficient. Consequently, to avoid Auger recombination it is necessary to produce as much radiative output as possible by operating the LED at low injected carrier concentration. This in turn means that the residual carrier concentration must be kept low and therefore it is essential to remove un-intentional impurities and native lattice defects. It would appear that the use of Pb as a neutral

solvent is highly effective in this respect. By using Pb neutral solvent together with Yb in p-i-n heterojunction LEDs it is possible to achieve an increase in 300 K output power of about a factor of 10.

3 High Pressure Measurements

Hydrostatic pressure has been extensively used to study the recombination mechanisms that occur in semiconductor LEDs and laser structures[72]. But, although the technique has been widely used to study visible and near infrared emitters, its application to sources operating at wavelengths beyond 2 μm has only recently been investigated. The application of hydrostatic pressure can give valuable information about the relative significance of the different recombination mechanisms that are sensitive to changes in the bandgap. To obtain information about the relative

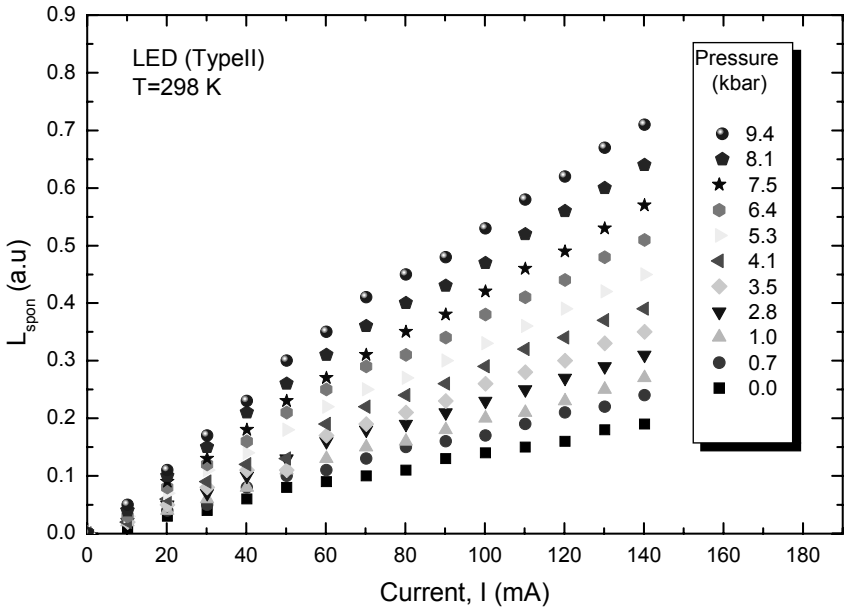

Figure 10. Measured integrated spontaneous emission intensity as a function of current for 0 kbar<*P*<9.4 kbar at room temperature for an InAs/InAsSbP 3.3 μm LED .

importance of SRH and Auger recombination in the mid-infrared, the behaviour of 3.3 μm and 3.8 μm LEDs, which had InAs or $InAs_{0.94}Sb_{0.06}$ in the active region, (giving type II and type I band line-ups respectively) has been investigated[72]. The devices were operated using a low duty cycle (typically 5%) in order to avoid Joule heating effects. The measurements were made at room temperature using a He hydrostatic pressure cell and 77 K InSb photodetector. Figure 10 shows a plot of the integrated spontaneous emission, corrected for detector response, against current in the pressure range 0 to 9.4 kbar, for one of the 3.3 μm LED samples after Yb purification of the active region. A significant increase in radiative efficiency of x 4 was observed for these type II diodes. Since the band offsets and the capture cross-section for SRH are almost independent of pressure it is clear that the increase in electroluminescence is associated with a reduction in Auger scattering.

One can account for the improvement in light output with hydrostatic pressure in these LEDs by considering the effect of pressure on the CHCC and CHSH Auger recombination processes. Simple analytical expressions can help to understand the variation of these processes with band-gap. The band-to-band Auger process can be expressed as a thermally activated process given by[73]:

$$C = C^0 \exp\left(\frac{-\Delta E_\alpha}{\kappa \mathrm{T}}\right) \Leftrightarrow \ln C = \ln C^0 - \frac{\Delta \mathrm{E}_\alpha}{\kappa \mathrm{T}}. \qquad (4)$$

Where C^0 is approximately independent of temperature and pressure, but includes the terms due to the coulomb interaction matrix between initial and final Auger states. The main pressure dependence of the Auger activation energy (ΔE_α) for the direct Auger recombination processes CHCC and CHSH is due to the bandgap dependence of ΔE_α and is given by[74]:

$$\Delta E_\alpha(CHCC) = \frac{m_e E_g}{(m_e + m_h)}, \quad \Delta E_\alpha(CHSH) = \frac{m_{so}(E_g - \Delta_{so})}{(2m_h + m_e - m_{so})}, \qquad (5)$$

where m_e ($0.023m_o$), m_h ($0.41m_o$) and m_{so} ($0.16m_o$) are the electron, hole and spin-orbit effective mass respectively (the values within the parenthesis are the effective masses of InAs at ambient conditions). Electron and spin-orbit effective masses, increase approximately in proportion with increasing pressure whilst the hole effective mass is relatively independent of pressure[72]. Δ_{so} is the spin-orbit split-off energy. It can be seen that the Auger coefficient reduces in significance with increasing E_g and hence with increasing pressure ($\frac{\partial \mathrm{E}_g}{\partial \mathrm{P}}$ for InAs is approximately 10 meV/kbar[75]). For longer wavelength devices the phonon-assisted Auger processes have activation energies much larger than the phonon energy and they are far less sensitive to the band structure and temperature compared to the band-to-band case[72]. Although in the InAs active region, the band gap and the spin–orbit band gap are nearly equal, experimentally no resonant behaviour in the light output as a function of applied hydrostatic pressure was observed.

Using this simplified model the bandgap dependence of ΔE_α and the bandgap dependence for the direct Auger recombination processes CHCC and CHSH can be

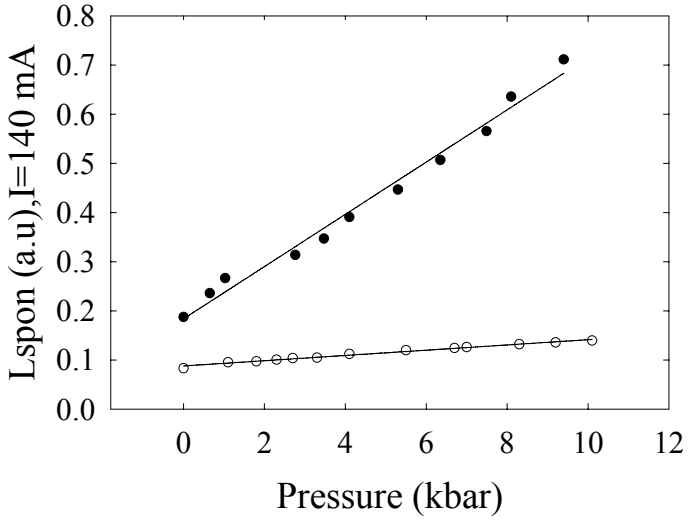

Figure 11. A comparison of the pressure dependence of the electroluminescence emission intensity for type-I (3.8 μm, open points), and type-II (3.3 μm, solid points) double heterostructure LEDs at 300 K. Reprinted with permission Copyright 2003 AIP [76].

calculated. Although both processes are reduced as a function of pressure the relative change for the CHSH process [a factor of 2.55 (2.55/3.74=68 %)] is much closer to the experimental change in light output (a factor of 3.74) than the change due to the CHCC process [a factor of 1.21 (1.21/3.74=32 %)]. Note that the total change due to CHSC+CHCC (a factor 3.76) is in excellent agreement with the experimental change in light output (a factor of 3.74). This suggests that CHSH is the dominant process in these devices from ambient up to the pressure range studied here. (According to these calculations the activation energies for the two processes became comparable at the highest pressure around 9.4 kbar). Note that inter-valence band absorption (IVBA) would also be reduced by de-tuning E_g above Δ_{so}, but this does not affect these measurements which were made viewing through the n-type side of the sample. It is worth mentioning that if radiative recombination dominates the device response, the output would reduce with increasing pressure due to reduction of the matrix element with increasing bandgap.

Figure 11 shows a plot of the light output at constant current (140 mA) as a function of applied hydrostatic pressure for the two samples together [76]. A factor of 1.7 increase in the light output for the type I, 3.8 μm LED (open points), and a factor of 3.96 for the type II, 3.3 μm LED (solid points) in the pressure range up to 10 kbar was obtained. There is clearly a much larger increase in electroluminescence from the type-II LED compared with the type-I LED. The 3.7 increase in the radiative efficiency of the type II LED compared to 1.7 in the case of the type I is an

experimental indication that Auger processes are more important for the type II LED compared to the type I LED. However, it is well known that the type II structure reduces the overlap between electron and hole wavefunctions since the carriers are delocalized. This should result in a reduction of the Auger coefficient C in type II structures compared to type I. But, these results indicate stronger Auger suppression with applied pressure for type II rather than type I structures. At first this seems anomalous, but the effective width of the recombination zone within the active region of the type II LED, ($d$eff) is significantly smaller, since the type II band edge alignment results in band bending and the injected carriers become localized near the interface. Therefore, the value of $d$eff is essentially determined by the carrier tunnelling distances, estimated as $d$eff ~150 Å. We suppose that, although type II recombination across the InAs/InAsSbP interface reduced the Auger coefficient C, the injected carrier concentration is actually greater than that found in the type I LED due to the small recombination volume localized near the interface. As Auger processes are strongly dependent on injected carrier concentration (~increase as n^3), the net result is an overall increase in the Auger rate (Cn^3). We may then interpret the larger increase in the light output as a function of pressure for the type-II LED compared to the type I LED as being associated with Auger suppression. In type II quantum wells the radiative and Auger recombination coefficients depend on the band gap as $B \sim Eg^2$ and $C \sim Eg^{-5.5}$ respectively, and at zero applied pressure, $B \sim 10^{-10}$ cm^3s^{-1} and $C \sim 8x10^{-27}$ cm^6s^{-1}. This gives the radiative contribution to the current density as 14% at P=0 and 40% at P =9.4 kbar. Simple estimates predict an increase of about 2.85 in light output when the pressure is increased from 0 to 9.4 kbar at constant current (I=140 mA). This is approximately in agreement with the value of 3.74 obtained experimentally.

3 Optical Extraction

In addition to the problems associated with radiative efficiency, mid-infrared LEDs also suffer from the problem of low optical extraction efficiency which is common to most LEDs as a result of the high refractive index (n~3.5) of the semiconductor material. This results in a small critical angle (~15^0) and a narrow escape cone such that the ratio of external to internal efficiency is $1/n(n+1)^2 \sim 1/70$. The LED structure employed must ensure that the majority of generated photons meet the emission surface within the critical angle and that the that these photons are transmitted to the emitting surface within a minimal path length to prevent absorption losses. In contrast to the work on improving internal radiative efficiency there has been surprisingly little research into solving this fundamental problem. The principal approaches have been to use immersion lenses, optical concentrators [77,78], surface texturing[79] or resonant cavity structures [80] to extract more light from the LED.

Although Bragg mirror technology has been extensively implemented in visible and near-IR resonant cavity LEDs (RC-LED)[81] and vertical cavity surface-emitting lasers (VCSELs), the technology has been slow to transfer out to the longer wavelengths. In general RC-LEDs exploit the properties of planar micro-cavities to

redirect a larger fraction of the spontaneous emission into the escape cone, thereby increasing the extraction efficiency and improving the spectral performance. Whereas VCSELs need highly reflective mirrors (i.e. >99%) the requirements for LED enhancement are much less stringent. In a resonant cavity LED (RCLED) the micro-cavity essentially clamps the linewidth and emission wavelength with respect to the LED drive current. The cavity mode and the semiconductor bandgap have opposite temperature sensitivity resulting in a much more stable emission wavelength. This is an important consideration for a practical gas sensor where the LED is tuned to the target gas absorption resonance and should remain fixed over the ambient operating range (-40^0C to $+50^0$C). RCLEDs are somewhat easier to work with than VCSELs because they need only a small Bragg period number (5-6) rather than 20-30 typically required for VCSELs. These LEDs can in principle provide some of the most important advantages of the VCSEL but without the corresponding stringent requirements on epitaxy. Potential performance advantages include; increased optical extraction (higher output power), improved spectral purity (narrow linewidth), directed emission and improved temperature stability. Modelling by De Neve et al [82] has shown that it is possible to obtain high external quantum efficiencies using low reflectivity mirrors. Some mid-infrared resonant cavity light emitting diodes (RCLEDs) based on CdHgTe alloys and grown by MBE have now been reported [83]. These devices contain a single Bragg mirror reflector and emit at 3.18 μm and 3.35μm. The reported spectral bandwidth (FWHM) is less than half that of the bulk active layer emission bandwidth and the device also has improved beam divergence characteristics. Application to III-V systems has been slow mainly due to epitaxial growth problems associated either with mismatch between DBR layers or between active region and DBR layers. However, powerful (>20mW cw) VCSELs operating at 2.2μm have been demonstrated [84].

InSb optical concentrators have been modelled and applied in a “Winston cone” configuration to effectively make the volume of the emitting material smaller while keeping the emission constant. Micro machining of a transparent n^+ - InSb substrate using sequential reactive ion etching with CH_4 : H_2 and O_2 was employed to increase the output of InSb/InAlSb LEDs. Optical gains of 3.5 over conventional mesas were obtained from the resulting large area ($3cm^2$) LED arrays. In the case of near IR GaAs LEDs, the problem is alleviated by depositing a lens shaped epoxy resin to aid index matching and increase the escape cone. Unfortunately this is inefficient for mid-IR LEDs since most inert epoxy resins have strong absorption in the 2-5μm region and fabrication of such index matching lenses in silicon is impractical. Silicon immersion micro lenses have been used for detector arrays but with limited effect due to contact and alignment problems[85]. This technique has however been successfully implemented for HgCdTe LEDs using a CdZnTe coupling lens, such that 20% of the available light could be extracted. Matveev et al[86] used a similar approach for InAsSb, but employed selective chemical etching to produce a device with a 30μm deep inverted mesa and a silicon sub-mount to produce an emitting surface free of contact pads and bond wires, giving a peak output of 60μW at 5.5μm using 1A pulses (1.5% duty cycle).

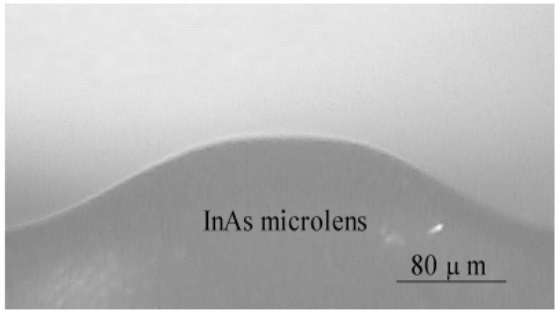

Figure 12. Cross-section of an integral micro lens etched into the substrate on the back of an InAs LED

Another potentially useful approach for mid-infrared optoelectronic devices is an InAs micro lens, integrated onto the radiation emitting chip. The LED is fabricated and mounted in the epi-side down configuration with the lens etched into the substrate on the opposite side. To achieve the necessary diameter the micro lens production process involves first etching a ring into the substrate and then shaping the surface using an isotropic etchant. The final shape is strongly affected by the original ring diameter and depth. Using a ring diameter of 650μm and a deep groove, it is possible to produce an integral lens as shown in Fig. 12. Optical modeling using ray-tracing software has shown that even though the refractive index is high, the lens needs to be quite thick before it has a significant effect on extraction. The usual 500 μm substrate thickness of readily available InAs effectively places an upper limit on this and reduces the benefits of these lenses. Further increases can be obtained by defining a small spot for the emission region and etching a mesa to act as a "corner reflector". However, in practice this has so far not resulted in more than a factor of 2 improvement in extraction efficiency compared with a conventional surface emitting mesa.

4. Comparison of Devices

Comparing the performance of LEDs at different wavelengths in the 2-5 μm spectral range reveals that the output power and associated quantum efficiency decreases with increasing wavelength. This observation is generally consistent with a decreasing spontaneous emission rate which decreases as the alloy bandgap decreases. The temperature dependence of emission intensity is determined by the competing non-radiative recombination processes, and in InAs alloys primarily through the Auger mechanisms[87,88] CHCC and CHSH, which have a stronger (exponential) temperature dependence than the spontaneous recombination coefficient. A plot of the temperature quenching of the electroluminescence emission from different LEDs made in our laboratory and normalised to 1.0 at 77 K is shown in figure 13.

The devices all showed generally similar behaviour, but the 3.8μm LED exhibited the least severe reduction in electroluminescence on approaching room temperature, while the 3.3μm and 4.6μm LEDs were almost the same. We may estimate the Auger coefficient in the active region of these LEDs and its temperature dependence by fitting our experimental data. Because in each case the active region has been purified, we are able to make the assumption that non-

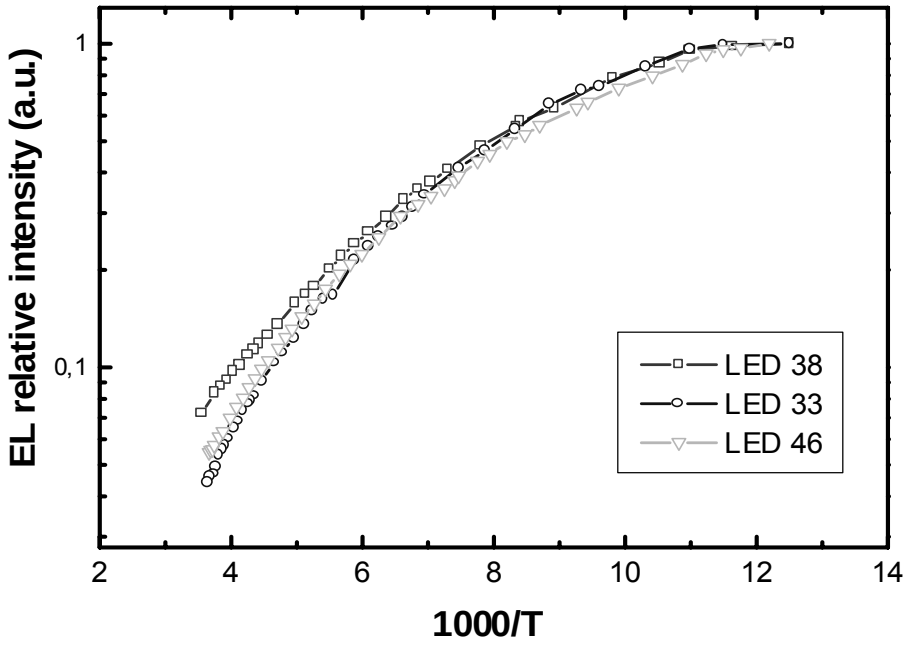

Figure 13. A comparison of the normalised temperature dependence of electroluminescence emission intensity of 3.3, 3.8 and 4.6 μm LEDs over the temperature range 77-300 K (after Krier *et al.*)

radiative band-to-trap recombination can be neglected, to a first approximation. The temperature dependence of B is known to be of the form $B(T)=B_0(T_r/T)$ [89] and T_r was set to 30K, with $B_0 = 2\times10^{-10}$ cm^3s^{-1}. The temperature dependence of C was assumed to be exponential and of the form $C(T)=C_0\exp(-E_\alpha/kT)$ [90], where E_α is the activation energy for Auger recombination and C_0 is the Auger coefficient. A reasonably good fit to the data was obtained when $C_0=1.5\times10^{-26}$ cm^6s^{-1} and E_α=31 meV, implying that C = 1.35×10^{-28} cm^6s^{-1} at 77K and 4.5×10^{-27} cm^6s^{-1} at 300K respectively. The values of Auger coefficient, $C_0=1.5\times10^{-26}$ cm^6s^{-1} and activation

energy, E_α=31meV are generally in good agreement with those obtained previously by other workers.[49,87].

In the 3.8μm LED the bandgap energy (E_g = 0.314eV) is less than the split-off band gap energy (Δ_{so} = 0.347eV) at room temperature and the detuning may reduce non-radiative CHSH Auger recombination compared with the 3.3μm LED in which there is a near resonance. However, the 3.3μm LED is overall brighter because of the higher spontaneous emission rate and because the recombination is type II across the InAs/InAsSbP interface as described earlier. We also consider that the type II nature of the recombination in the 3.3μm LED is producing some Auger suppression. In the 3.8μm LED, which has a type I heterointerface, the temperature at which $E_g = \Delta_{so}$ resonance occurs is estimated to be near 160K. But as is evident from figure 13, we failed to observe any pronounced reduction in EL emission intensity at this temperature in our experiment. This indicates that CHSH may not be the dominant non-radiative recombination mechanism in these LEDs and CHCC may be more important instead, which is consistent with recombination in an n-type active region. Indeed it may be that CHCC alone is responsible for the temperature quenching which we observed in each of the LEDs, (since they all have n-type active regions). In the 4.6μm LED there is an even larger difference between E_g (= 0.267eV) and Δ_{so} (= 0.311eV), yet the output power is lower than for the 3.8μm LED and in this case we attribute this partly to the higher net strain (~0.5%) present in the active region, which is also type I. This latter LED also has a strain-relaxed buffer layer to help accommodate the total strain of ~1% from the InAs substrate and although partly effective we consider that the 4.6μm LED has the highest concentration of Shockley-Read non-radiative recombination centres of the devices which we have fabricated to date.

5. InAsSb Quantum Dot Light Emitting Diodes Grown by Liquid Phase Epitaxy

There is currently much interest in the epitaxial growth and optical properties of quantum dots (QDs) for optoelectronic device applications because the zero dimensional properties of QDs could provide a means to suppress Auger recombination. In recent years, InSb, GaSb, AlSb and InAs QDs have been grown on GaSb and GaAs substrates by molecular beam epitaxy (MBE) or metal-organic vapour phase epitaxy (MOVPE). The resulting photoluminescence (PL) and electroluminescence (EL) from these QDs were however observed in the near infrared.[91,92,93,94,95,96,97,98,99]. By comparison there have been very few, reports of InSb or $InAs_{1-x}Sb_x$ QDs exhibiting emission in the spectral range beyond 2 μm. Recently, photoluminescence from $InAs_{1-x}Sb_x$ QD in the mid-infrared near 4 μm has been obtained[100] leading to the first observation of EL from $InAs_{0.75}Sb_{0.25}$ QD light emitting diodes. The samples were grown from the liquid phase using a modified (rapid slider) liquid phase epitaxy technique, as described previously elsewhere, and

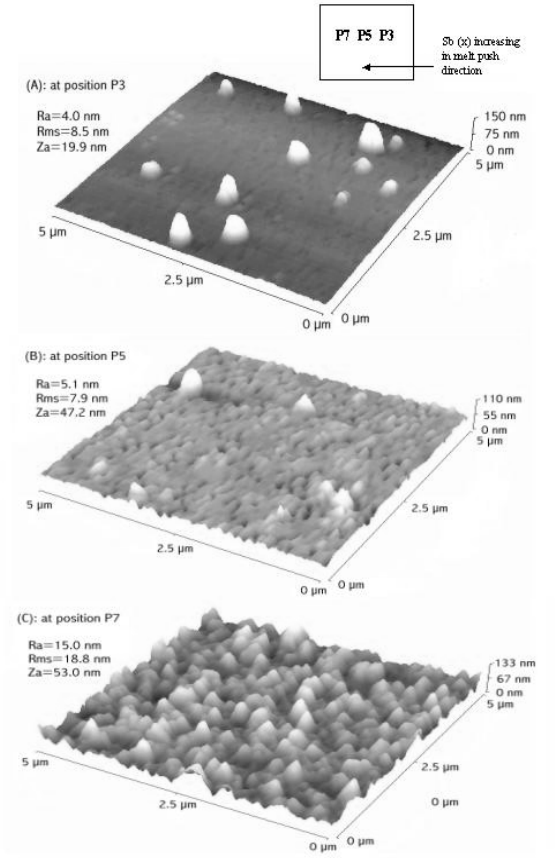

Figure 14. The AFM images obtained from un-encapsulated InAs $_{1-x}$ Sb $_{x}$ quantum dots with increasing Sb composition grown by LPE and corresponding to the passing direction of the melt across the substrate. Approximate compositions are A (x=0.20); B (x=0.25); and C (x=0.30) Reprinted with permission. Copyright 2000. American Institute of Physics

which is capable of producing quantum wells (QWs) and QDs. Essentially a linear motor is employed to rapidly wipe a thin slit of supersaturated melt over the substrate resulting in melt-substrate contact times as short as 0.5 ms. Under lattice matched growth conditions, continuous ultra thin layers or QWs are obtained, but when highly mismatched, self-assembled QDs are produced instead.

Figure 14 shows an AFM image of $InAs_{1-x}Sb_x$ QD with x~0.25 grown sandwiched between undoped (n-type) InAs encapsulation layers which were each 1 µm in thickness. The $InAs_{1-x}Sb_x$ QD layer was grown using a 0.6 ms contact time and 20 ^{o}C melt supercooling. After growth of the active region the sample was removed from the reactor and a PL characterisation of the encapsulated dots was made. The sample was reloaded and a 1 µm thick p^+ (Zn doped $2x10^{18}$ cm^{-3}) contact layer was re-grown at 455 ^{o}C. The sample was then processed into 375 µm diameter mesa-etched LEDs for EL measurements. A pulse current with 50 % duty cycle at 315 Hz was used to excite EL in the LED.

Figure 15 shows the 4 K EL spectrum obtained from an InAsSb QD LED using 250 mA injection current. The broad peak in the region near 4 μm is due to QD related transitions, the large FWHM being related to the inhomogeneous broadening from

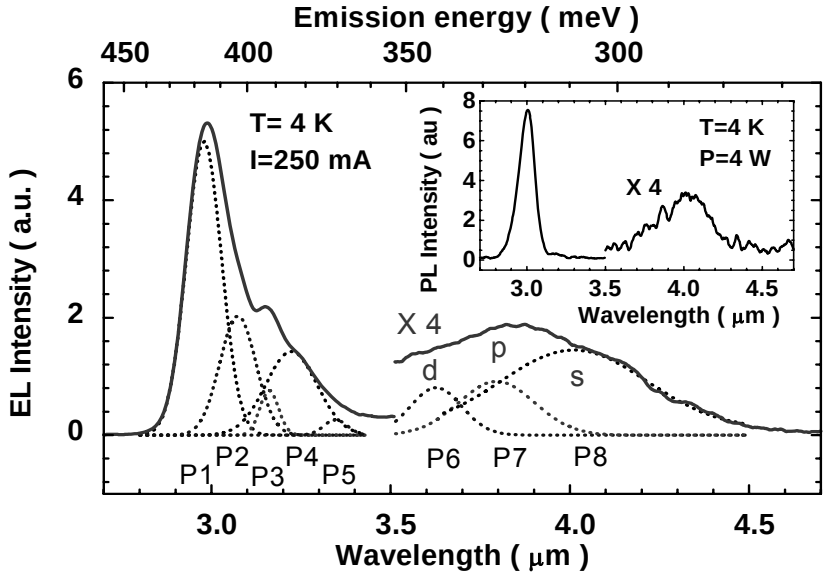

Figure 15. The electroluminescence emission spectrum obtained from an InAsSb quantum dot LED measured at 4 K using 250 mA injection current. De-convolution reveals the s,p,d confined state transitions of the QD. The inset shows the PL spectrum at 4 K for comparison. Reprinted from A. Krier, X-L Huang, Physica E, 15, 159 (2002) with permission from Elsevier

their size distribution. By using Gaussian line shapes for fitting, 3 peaks (P6, P7, P8) can be de-convoluted from the spectrum, which are attributed to recombination involving confined hole states in the QD[101]. The peaks P1(2.98 μm), P2(3.08μm) and P4(3.24μm) can be assigned to characteristic recombination in the InAs encapsulation based on previously observed results in the literature[13,14].

A schematic energy diagram of the type II $InAs_{1-x}Sb_x$ /InAs QD system is shown in Fig. 16. In bulk or epitaxial InAs, transitions involving a shallow donor level E_S and acceptors, E_{A1}, E_{A2} are normally observed in PL spectroscopy.[102,103,104,105,106]. Additional deep states are sometimes also observed in non-stoichiometric material or in samples containing strain. The broad band can readily be assigned to transitions originating within the quantum dot in good agreement with PL spectroscopy, as shown in the inset of Fig. 15, where the 4 K PL peak related to the $InAs_{0.75}Sb_{0.25}$ QD in the active region of the sample was also centred at 4 μm with a full width at half maximum (FWHM) of 400nm. We note that the QD emission is

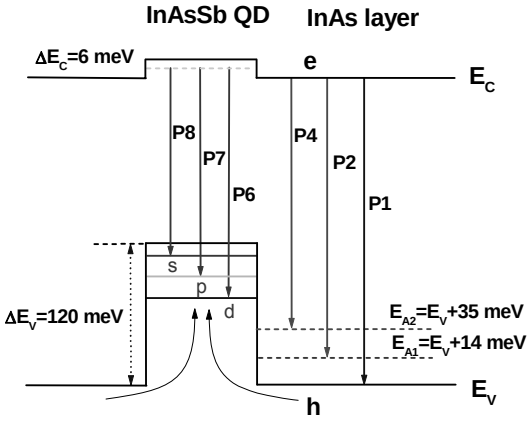

Figure 16. A schematic energy diagram of the type II $InAs_{1-x}Sb_x/InAs$ encapsulated quantum dot.

wider in EL than in PL due to the higher carrier injection level, which suggests that more QD sub-levels are populated. As the injection level is increased, Pauli blocking causes a saturation of the carrier number in lower energy states inside the QD and the relaxation rate from higher states decreases leading to observable emission from the excited levels. Two additional peaks P3 (3.16 μm) and P5 (3.33 μm) are associated with a thin wetting layer or a strained InAs layer covering the InAsSb QD. These peaks are more prominent in the EL than in the PL spectra and indicate the onset of the phonon bottleneck effect in these structures.

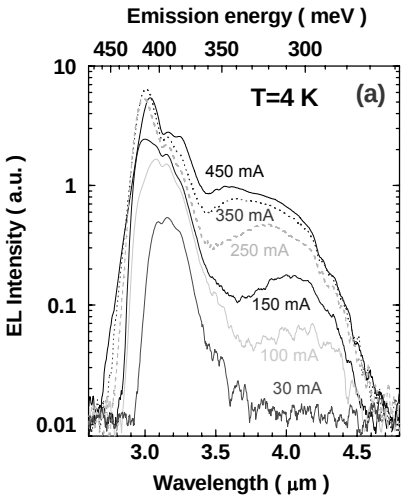

Figure 17. The 4 K EL spectrum of the QD LED at various injection currents Reprinted from A. Krier, X-L Huang, Physica E, **15**, 159 (2002) with permission from Elsevier

Figure 17 shows the quantum dot LED emission spectra and their dependence on injection current at 4K. It is evident that at 30mA there is essentially no QD emission and the injection has to be increased to 100mA before any significant QD emission is observable. This is evidence of the phonon bottleneck where there are insufficient phonons available to scatter holes into the deep QD potential and the

dots can become populated essentially only by Auger scattering which becomes significant at high carrier densities. The intensity of the QD electroluminescence at 4K was found to increase rapidly with increasing current relative to the InAs encapsulation. A blue shift was observed for the QD emission band as the current increased from 100 to 450 mA, due to the small density of states in the QD. In contrast, the InAs encapsulation shows no such shift. As the injection current increases, the intensity of the QD emission increases relative to the InAs-related transitions (P1,P2). Figure 18 shows the EL spectra at various temperatures in the range from 5 to 300 K. The intensity of the QD emission band increases as the temperature is increased from 5 to 30 K, before decreasing with the band-band recombination (P1). It was also observed that as the temperature was increased the minimum injection current for observable QD emission decreased, and for a fixed injection level the optimum QD EL intensity was obtained near 50K as shown in the inset of fig. 18. For each of the individual QD levels there exists a competition between thermal activation, carrier relaxation and radiative recombination. The details of the observed EL emission spectra depend on the balance between these processes. Assuming that the LED is operating in the phonon bottleneck regime at low temperature, and that the QD ground state is populated mainly by Auger recombination, then it is conceivable that as the temperature is increased the QD electroluminescence will increase in intensity as the phonon population increases.

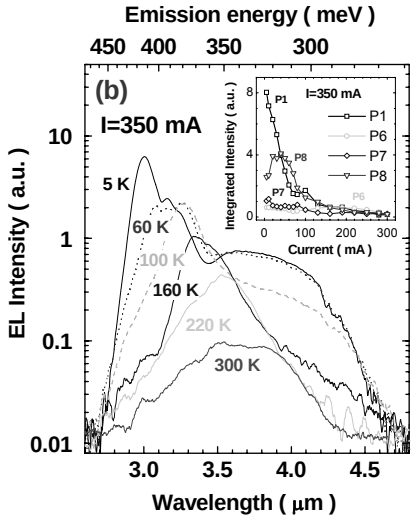

Figure 18. The integrated EL intensity dependence on temperature at 350 mA injection current. Reprinted from A. Krier, X-L Huang, Physica E, **15**, 159 (2002) with permission from Elsevier

Then, as the temperature approaches 100 K, holes are released by thermal activation or perhaps via tunnelling. Nevertheless, from examination of fig. 18 it is evident that at 300 K the InAs related transitions are mostly quenched whereas the QD EL persists up to room temperature. This result is encouraging since although these LEDs are not optimised and consist only of a p-i-n structure with a single layer of QDs in the active region, they compare quite favourably with previous work on 4.6 μm InAsSb LEDs.

6. Superluminescence and Ring Lasers

The increase in optical output power in the above investigations has come about largely through a careful reduction of the residual carrier concentration in the active region of mesa-etched LEDs with a central dot contact. By employing a ring contact it is possible to further increase output and to observe superluminescence from mid-infrared LEDs.

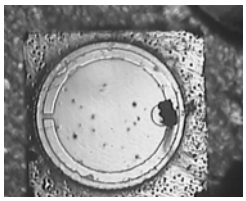

Figure 19. Nomarski microscope photograph of a typical mesa etched LED (350 μm diameter) with ring contact electrode (30 μm wide).

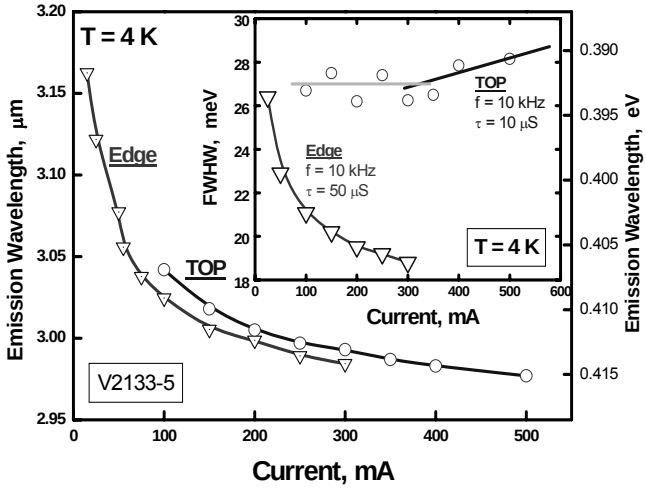

Figure 20. The current tuning behaviour of peak emission wavelength for edge and surface (Top) emission from the LED measured at 4K at a frequency of 10 kHz using 50 % duty cycle (50 μs pulses). The inset shows the corresponding FWHM variation with current, (duty cycle reduced to 10% at highest current to control Joule heating) .

A Nomarski microscope photograph of a typical mesa-etched LED chip produced with such a ring electrode is shown in figure 19. The corresponding back contact was deposited over the entire rear surface of the chip. The full-width at half-maximum (FWHM) of the resulting output from the top and from the edge of the LED is compared in figure 20. At 300K the electroluminescence peaks near 4.6μm, making these emitters suitable for use in the environmental monitoring of carbon monoxide. By using similar ring electrodes on LED structures with InAs active regions (as described earlier) it is possible to obtain superluminescence at 3.3 μm.

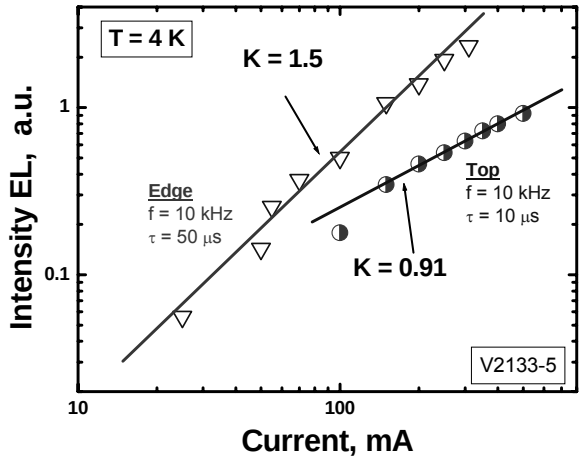

Figure 21. The light–current characteristics measured from the surface and edge of the ring geometry LED at 4K

Due to current crowding effects the ring contact produces a whispering gallery mode as injection current is increased, resulting in superluminescence at room temperature and increased optical output. The electroluminescence emission spectra measured from the edge of the ring contact LED exhibit spectral line narrowing with increasing injection current [107]. The halfwidth (FWHM) at 15 mA is 880 nm whereas at 100 mA it is only 580 nm. The ratio of these halfwidths is 1.51 and shows that the device is a superluminescent diode. The light–current characteristics for surface and edge emission are compared in Fig. 21. Both the curves have a linear portion in the current range from 0.015 to 0.3 A. The corresponding slopes were determined to be 1.5 for the edge radiation and 0.91 for the top radiation. A value of the slope of the light–current characteristic which is greater than 1 is further evidence for superluminescence (for edge radiation) in these LEDs.

Following the observation of superluminescence at 3.3μm and 4.6μm due to the high Q arising from total internal reflection in LEDs with a ring contact configuration, further optimisation led to the demonstration of the first mid-infrared ring laser operating near 3 μm at 80 K as shown in the electroluminescence spectrum of figure 22[108].

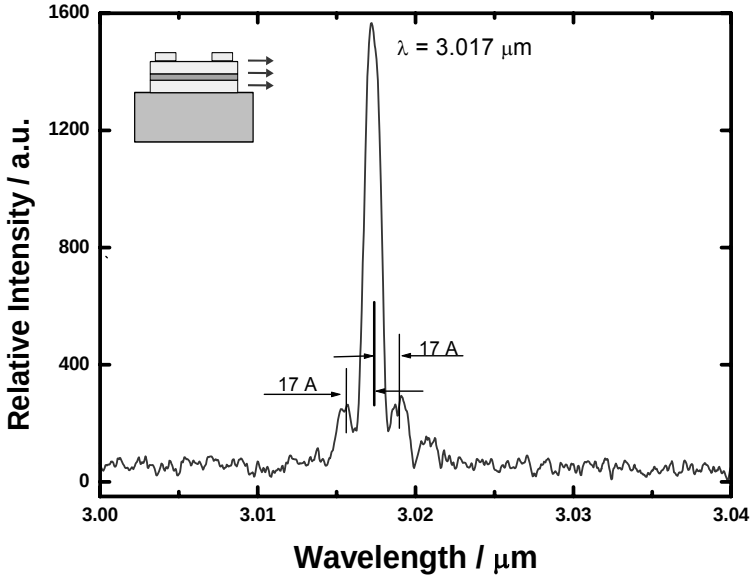

Figure 22. The mode spectrum obtained at 80 K from a mid-infrared whispering gallery mode ring laser .

Similar optical resonant mode behavior has been observed in microdisk lasers[109,110] and light emitting diodes operating at much shorter wavelengths[111,112]. It has been shown that a microdisk cavity may support two different resonant mode types, radial and whispering gallery modes (WG) [113]. Radial modes are dominated by photon wave motion along the radial direction of the disk, the equivalent cavity being formed between the edge and the centre of the disk. These radial oscillations are unlikely in this case due to the ring contact and local current crowding which prevents such propagation. The WG mode, on the other hand, may be thought of as in-plane propagation around the inside perimeter of the mesa, which is facilitated by total internal reflection. The modes are solutions of the three-dimensional Maxwell equations. However, assuming that the radiation is effectively confined vertically within the active region of the mesa, then we may approximate this situation using a two dimensional solution which yields Bessel functions for the radial field distribution. The effective cavity length of $2\pi R$ imposed by the periodic boundary condition on the circulating wave results in the WG eigenmode condition: $2\pi Rn = m\lambda$

for large integer *m*, where *R* is the mesa radius, *n* is the refractive index, and the mode spacing is given by $\Delta\lambda_{WG} = \lambda^2/2\pi Rn$. This enables us to estimate a WG mode spacing of 2.1 nm, which agrees reasonably with the value of 1.7nm measured experimentally from the spectra of Fig. 22. Although the device had no intentional output coupler, coherent output was obtained, most likely due to light scattering from imperfections on the mesa edge of the ring waveguide. The laser exhibited a characteristic temperature of T_0 = 25 K with a maximum operating temperature of 125 K. Consequently, with proper design of the output coupler, further improvements in the laser operating temperature and threshold current can be expected.

Conclusion

The Physics and technology associated with the fabrication and operation of mid-infrared LEDs has been briefly reviewed. The fundamental difficulties associated with realising practical sources at different target wavelengths for gas analysis have been discussed. The principal limitations to performance in determining high output power at room temperature were identified to be quantum efficiency and optical extraction. Some of the different device designs and approaches used for the suppression of non-radiative Auger recombination and the reduction of Shockley-Read-Hall centres were described to establish an overview of the "state-of-the-art". Even though measurements at longer wavelengths are more challenging, the use of high applied pressure as an investigative tool has been shown to be very useful in identifying and understanding recombination mechanisms in mid-infrared LEDs. Liquid phase epitaxy continues to hold a strong position in mid-infrared LED technology and many of the current best LEDs have been fabricated using this technique. Furthermore, the use of rare earth gettering in LPE growth of InAs(Sb) LEDs has been established as an important technique. LED performance improvements were realised (a) by using rare earth gettering as a melt purification technique to reduce residual carrier concentration and (b) by use of type II interface heterostructures to obtain Auger suppression. LEDs which match some of the target wavelengths of special interest for gas detection, including 3.3μm (CH_4) and 4.6μm (CO) have been realised[114]. These emitters are poised to become useful components in the realisation of cost-effective practical instruments for the environmental monitoring of methane and carbon monoxide. The recent development of quantum dot LEDs and whispering gallery mode ring lasers for the mid-infrared also have interesting possibilities in this rapidly expanding field.

Acknowledgements
The authors wish to thank those colleagues who have made significant contributions to the work summarized in this chapter, especially H. Gao, Z. Labadi and S. Choulis. We are grateful to the Engineering and Physical Sciences Research Council (EPSRC) for providing the funding associated with this research. We also wish to thank The Royal Society and Kidde plc for supporting various aspects of the work.

References

[1] See for example : InAsSbP/InAs LEDs for the 3.3-5.5μm spectral range, B. Matveev et al, IEE Proc. Optoelectronics, **145,** Special Issue on Mid-IR devices & materials and papers therein – (see also vol **144** for additional related papers)

[2] High Power 4.6 μm LEDs for CO detection grown by LPE using rare earth gettering. A.Krier, H.Gao, V.Sherstnev, Yu.Yakovlev. Electronics Letters, (USA), **35**, 1665-7(1999)

[3] A.N.Baranov, A.N.Imenkov, O.P.Kapranchik, V.V.Negreskul, A.G.Chernyavskii, V.V.Sherstnev Yu.P.Yakovlev. Long-wavelength light-emitting diodes, based on InAsSbP/InAs heterostructures (λ=3.0-4.8μm) at 300K with wide-gap window. Pisma v Zhurnal Tekh.Fiziki (USSR), **16** (16), p.42-47, (1990).

[4] S. McCabe and B.D. MacCraith , *Electron.Lett.* **29** 1719–21(1993)

[5] S.D. Smith, A. Vass, P Bramley, J.G. Crowder and C.H. Wang, IEE proc-Optoelectronics, **144**, No 5, 266 (1997)

[6] M.K. Parry and A. Krier, *Electron. Lett.* **30** 1968–69 (1994)

[7] A.A. Popov, V.V.Sherstnev, Y.P. Yakovlev, A.N. Baranov and C. Alibert, *Electron. Lett.* **33** 86–88 (1997)

[8] A. Krier and Y. Mao, *IEE Proc.Optoelectron.* **144** 355–59 (1997).

[9]A.A. Popov , M.V Stepanov, V.V. Sherstnev and Y.P. Yakovlev, *Tech. Phys. Lett.* **24** 596–98 (1997)

[10] A. Krier & V.V. Sherstnev, J. Phys. D: Appl. Phys. **33**, 101-106 (2000) Powerful interface light emitting diodes for methane gas detection.

[11] A.A Popov, V.V. Sherstnev, Y.P. Yakovlev, A.N. Baranov and C.Alibert, 'Powerful mid-infrared light emitting diodes for pollution monitoring' Electr. Lett., **33** (1997) 86-88

[12] A.Krier and Y.Mao, '2.5μm light emitting diodes in $InAs_{0.36}Sb_{0.20}P_{0.44}$ /InAs for HF detection, IEE Proc Optoelectronics **144**, 355-359 (1997)

[13] Powerful 4.6μm light emitting diodes for CO detection, A. Krier, H.H. Gao, V.V. Sherstnev & Y. Yakovlev, - J. Phys D, **32** , 3117-3121 (1999)

[14] A.A Popov, M.V. Stepanov, V.V Sherstnev, Y. P. Yakovlev 'InAsSb light emitting diodes for the detection of CO_2
(λ=4.3μm)' Technical Phys. Lett., Vol **24**, No.8, 1998 p596-598

[15] A. Verdin, Gas Analysis Instrumentation, Wiley, New York, 1975

[16] I. Melngailis & R.H. Rediker, J. Appl. Phys, **37**,899(1966)

[17] I. Melngailis & R.H. Rediker, Appl. Phys. Lett., **2**,202 (1963)

[18] O. Madelung, Physics of III-V compounds, Wiley, New York, 1964

[19] A. Andreev et al, Sov. Techn. Phys Lett., **16**, 135-137(1990) Semicond. **27**, 236-240 (1993)

[20] N. P. Esina et al, J . Appl. Spectrosc**. 42**, 1985, 7465

[21] A.A Popov, V.V. Sherstnev, Y.P. Yakovlev, 1.94μm LEDs for moisture content measurements, Tech. Phys. Lett., **23**, 783 (1997)

[22] H.H. Gao, A. Krier and V.V. Shertsnev, J. Phys. D – Appl. Phys. **32** (1999) 1768-1772

[23] A. Krier, V.V. Sherstnev & H.H. Gao, A novel LED module for the detection of H_2S at 3.8 μm, J. Phys. D.-Applied Phyiscs, **33**, 1656, (2000)

[24] PJP Tang et al, Appl. Phys. Lett., 72,3473 (1998) efficient 300K light emitting diodes at λ = 5μm and 8μm from inAs/InasSb single quantum wells.

[25] M.J. Pullin et al., Appl. Phys. Lett., 74, 2384 (1999) Room temperature InAsSb strained-layer superlattice light emitting diodes at 4.2μm with AlSb barriers for improved carrier confinement

[26] C. Sirtori et al., Appl. Phys. Lett., 66., 4, (1995) Quantum cascade unipolar intersubband light emitting diodes in the 8-13μm wavelength region

[27] J. Faist et al, Appl. Phys. Lett.,64,1144 (1994)

[28] J. Faist et al, Appl. Phys. Lett., 65,94(1994)
[29] T. Ashley, C.T. Elliott, N.T. Gordon, R.S. Hall, A.D. Johnson & G.J. Pryce, Appl. Phys. Lett.,**64**, 2433(1994)
[30] T. Ashley, N.T. Gordon & T.J. Phillips, J. Modern Optics, 46, 1677 (1999) Optical modelling of cone concentrators for positive and negative IR emitters.
[31] T. Ashley & C.T. Elliott, Electron. Lett., 21, 451 (1985)
[32] T. Ashley, C.T. Elliott, N.T. Gordon, R.S. Hall, A.D. Johnson & G.J. Pryce, Infrared Phys & Technol., **36**, 1037 (1996)
[33] T. Ashley, C.T. Elliott, N.T. Gordon, R.S. Hall, A.D. Johnson & G.J. Pryce, J. Crystal growth, 159, 1100 (1996)
- see also paper in this issue.
[34] C. Verie & C.R. Granger, Acad. Sci. Paris, **261**, 3349 (1965)
[35] K.K. Mahavadi et al, J. Vac. Sci. & Tecjhnol., A 8, 1210 (1990)
[36] A. Ravid &A. Zussman , G. Cinader & A. Oron, Appl. Phys. Lett., 55, 2704 (1989)
[37] R. Zucca et al, J. Vac. Sci. & Technol., A 6, 2725 (1988).
[38] P. Bouchut et al., J. Vac. Sci. & Technol.,B9, 1794 (1991)
[39] T. Ashley, C.T. Elliott, N.T. Gordon, R.S. Hall, C.D. Maxey & B.E. Matthews, Appl. Phys. Lett. **65**, 2314 (1994)
[40] W. Lo & D.E. Swets, Appl. Phys. Lett., **36**, 450 (1980)
[41] Z. Shi et al, Appl. Phys Lett., **66**, 2573 (1995)
[42] Xu J, Lambrecht A, Tacke M**,** IEEE PHOTONIC TECH L **10**: (2) 206-208 FEB 1998
[43] Feit Z, Mak P, Woods R, et al. SPECTROCHIM ACTA A 52: (8) 851-855 JUL 30 1996

[44] C.R. Pidgeon et al, Phys Rev. B. **58**, 12908 (1998)
[45] Z. Shi, Appl. Phys. Lett., **72**, 1272 (1998)
[46] T. Ashley et al, Appl. Phys. Lett., **64,** 2433 (1994) and T. Ashley 7 C.T. Elliott, Semicond. Sci & Technol. **6**, C99 (1991)
[47] M.J. Kane et al, Mater. Res. Soc. Symp.Proc. **450**, 129 (1997)
[48] A.R. Beattie, J. Phys. Chem. Solids, 23, 1049 (1962).
[49] M.Kane et al, "Emission efficiency in InAs LEDs controlled by surface recombination" Presented at Boston **MRS** conference (Dec 1996)
[50] M.J. Kane et al, Appl. Phys. Lett., **76**, 943 (2000)
[51] M. Takeshima, Auger recombination in InAs , Jap. J. Appl. Physics 22, 491,(1983)
[52] See for example; A.N.Baranov, T.I.Voronina, T.S.Logunova, M.A.Sipovskaya, V.V.Sherstnev, Yu.P.Yakovlev. Semiconductors, 27, (1993). Zotova NV, Karandashev SA, Matveev BA, et al. Semiconductors, *33,* 920, (1999).
A.Krier, H.H.Gao, V.V.Sherstnev. Journal of Applied Physics, 85, 8419, (1999). A.Krier, V.V.Sherstnev. Journal of Physics D (Appl. Phys), 33, 101, (2000).
[53] A.Krier, V.V. Sherstnev, Yu.Yakovlev. Journal of Applied Physics, **33**, 101, (2000).
[54] A.Kumar, D.Pal & D.N. Bose, J. Electronic Mater., **24**, (1995) 833
[55] M. C. Wu et al., J. Appl. Phys. **71**(1) 1992, 456
[56] W. Gao et al., J. Appl. Phys. **80**(12) 1996, 7094
[57] N.T. Bagraev, L.S. Vlasenko, K.A. Gatsoev, A.T. Gorelenok, A.V. Kamanin, V.V. Mamutin, B.V. Pushnyul, V.K. Tibilov, Y.P. Tolparov and A.E. Shubin , Sov. Phys.-Semiconductors **18** (49) 1984
[58] F. Bantien, E. Bauser & J. Weber, "Incorporation of erbium in GaAs by liquid phase epitaxy", J. Appl. Phys.,61,(1987)2803

[59] Purification of epitaxial InAs grown by liquid phase epitaxy using gadolinium gettering, A. Krier, H.H. Gao & V. Sherstnev, J. Appl. Phys., **85**,(12) 8419-8422 (1999).
[60] High quality InAs grown by liquid phase epitaxy using gadolinium gettering, H.Gao, A. Krier & V. Sherstnev, Semicond. Sci & Technol. 14, 441-5 (1999), IOP Publishing
[61] N.V. Zotova et al., The first intenational conference on mid-optoeletronics materials and devices, Lancaster, 1996
[62] R. D. Grober , et al., Physics Review B, vol. **43**, No. 14, 1991, 11732
[63] Z.M.Fang, et al., J.Appl. Phys. **67**(11), 1990, 7034
[64] Y.Lacroix, et al., Appl. Phys. Lett. **66**(9) 1995, 1101
[65] R. D. Grober et al., J. Appl. Phys**. 65**(10) 1989, 4079
[66] P.J.P Tang, et al., Semicond. Sci. Technol**. 8**, 1983, 2135
[67] H.H. Gao, A. Krier and V.V. Shertsnev, J. Phys. D – Appl. Phys. **32** (1999) 1768-1772
[68] S.Kim, M.Erdtmann, D.Wu, E.Kass, H.Yi,J.Diaz, and M.Razeghi, Photoluminescence study of InAsSb/InAsSbP heterostructures grown by low-pressure metalorganic chemical vapor deposition. Appl.Phys.Letters **69** (11), pp. 1614-1616 (199b).
[69] A. Krier, H.H. Gao, V.V. Sherstnev & Y. Yakovlev, High Power 4.6μm light emitting diodes for CO detection, J. Phys D, **32** , 3117-3121 (1999), IOP Publishing
[70] A.N.Baranov, T.I.Voronina, A.A.Gorelenok, T.S.Logunova, A.M.Litvak, M.A.Sipovskaya, S.P.Starosel'tseva, V.A.Tikhomirova, V.V.Sherstnev, Yu.P.Yakovlev. Semiconductors, **26**, 905, (1992).
[71] A.Krier, V.V. Sherstnev, The influence of melt purification and structure defects on mid-infrared light emitting diodes, J. Phys. D-Applied Physics, **36** (13), 1484, 2003, IOP Publishing
[72] S.A. Choulis, A. Andreev, M. Merrick, S. Jin, D.G. Clarke, B.N. Murdin, A.R. Adams, A. Krier, V.V. Sherstnev, Phys. Stat. Sol. B- Basic Research. **235**(2), 312 (2003), John Wiley
[73] A. R. Adams, M. Silver, and J. Allam, *Semiconductors and Semimetals*,Vol. 55, Academic, London, (1998),
pp. 301–331.
[74] G. G. Zegrya and A. D. Andreev, JETP **82**, 328, (1996).
[75] G. G. Zegrya and A. D. Andreev, Appl. Phys. Lett. **67**, 2681, (1995).
[76] S.A. Choulis, A. Andreev, M. Merrick, , A.R. Adams, B.N. Murdin, A. Krier, V.V. Sherstnev, Appl. Phys. Lett, 82(8), 1149 (2003), American Institue of Physics
[77] T. Ashley, D.T. Dutton, C.T. Elliott, N.T. Gordon & T.J. Phillips, SPIE conference 3289 "Micro-optics Integration and assemblies" part of Photonics West meeting, San Jose, CA, USA, 26-30 Jan 1998
[78] T. Ashley, N.T. Gordon & T.J. Phillips, J. modern Optics, 46 (11), 1677 (1999)
[79] I. Schnitzer et al, Appl. Phys. Lett., **63**, 2174 (1993)
[80] Hadji E. et.al.: Resonant cavity light emitting diodes for the 3-5μm range, *Solid-State Electronics*, Vol. 40, pp.473-6, 1996
[81] P.N. Stavrinou et al, J. Appl. Phys., 86,3475 (1999)
[82] H. De Neve et al, Impact of planar microcavity effects on light extraction - Part I: Basic concepts and analytical trends , IEEE J Quantum Elect **34**: (9) 1612-1631 (1998)

[83] Hadji E. et.al.: Resonant cavity light emitting diodes for the 3-5μm range, *Solid-State Electronics*, Vol. **40**, pp.473-6, 1996
[84] Baranov AN, Rouillard Y, Boissier G, et al. Electron Lett 34: (3) 281-282 FEB 5 1998
[85] N.T. Gordon, C.L. Jones & D.J. Purdy, Infrared Physics., 31, 599 (1991)
[86] B. Matveev et al, IEE Proc. Optoelectronics **145**, 254 (1998)
[87] A. Sugimura, "Band to band Auger effect in GaSb and InAs lasers", J. Appl. Phys. Vol.**51**, No.8,pp4405-4411(1980).
[88] M. Takeshima, "Disorder-enhanced Auger recombination in III-V alloys" J. Appl. Phys. Vol.**49**, No12, pp6118-6124.(1978)
[89] S. Chinn, P. Zory, and A. Reisinger, IEEE J. Quantum Electron., **QE-24** 2191 (1988)
[90] B. Gel'mont, Z.Sokolova, and I. Yassievich, Sov. Phys. Semicond. **16**, 382 (1982)
[91] E. R. Glaser, B. R. Bennett, B. V. Shanabrook, and R. Magno, Appl. Phys. Lett. **68**, 3614 (1996).
[92] G. Park, O. B. Shchekin, d. L. Huffaker, and D. G. Deppe, Appl. Phys. Lett. **73**, 3351 (1998).
[93] E. Alphandery, R. J. Nicholas, N. J. Mason, B. Zhang, P. Mock, and G. R. booker, Appl. Phys. Lett. **74**, 2041 (1999).
[94] A. Krier, Z. Labadi, and A. Hammiche, J Phys D: Appl. Phys. **32**, 2587 (1999).
[95] K. Mukai, N. Ohtsuka, H. Shoji, and M. Sugawara, Appl. Phys. Lett. **68**, 3013 (1996).
[96] S. Raymond, P. Hawrylak, C. Gould, S. Fafard, A. Sachrajda, M. Potemski, a. Wojs, S. Charbonneau, D. Leonard, P. M. Petroff, and J. L. Merz, Solid State Commun. **101**, 883 (1997).
[97] Raymond, X. Guo, J. K. Merz, and S. Fafard, Phys. Rev. B, **59**, 7624 (1999).
[98] S. Fafard, Appl. Phys. Lett. **76**, 2707 (2000).
[99] J. Oswald, K. Kuldová, J. Zeman, E. Hulicius, S. Jullian, and M. Potemski, Materials Science and Engineering B, **69-70**, 318 (2000).
[100] A. Krier, X. L. Huang, and A. Hammiche, Appl. Phys. Lett. **77**, 3791 (2000)American Institute of Physics
[101] A. Krier, X-L Huang, Physica E, **15**, 159 (2002)
[102] P. J. P. Tang, C. C. Philips, and R. A. Stradling, Semicond. Sci. Technol. **8**, 2135 (1993).
[103] P. J. P. Tang, M. J. Pullin, S. J. Chung, C. C. Phillips, R. A. Stradling, A. G. Norman, Y. B. Li, and L. Hart, Semicond. Sci. Technol. **10**, 1177 (1995).
[104] R. Grober & H.D. Drew, J. Appl. Phys. **65**, 4079 (1989)
[105] S. H. Wei, and A. Zunger, Phys. Rev. B, **52**, 12039 (1995).
[106] Y. B. Li, D. J. Bain, L. Hart, M. Livingstone, C. M. Ciesla, M. J. Pullin, P. J. 10. Tang, W. T. Yuen, I. Galbraith, C. C. Phillips, C. R. Pidgeon, and R. A. Stradling, Phys. Rev. B, **55**, 4589 (1997).
[107] V.V. Sherstnev, A. Krier, G. Hill, High tunability and superluminescence in InAs mid infrared light emitting diodes, J. Appl. Phys. D - Applied Physics, **35**, 196, (2002) IOP Publishing
[108] A. Krier, V.V. Sherstnev, D. Wright, A.M. Monakhov, G. Hill, Electron. Lett., **39**(12), 916 (2003) IEE
[109] S.A. Backes, J.R.A. Cleaver, A.P. Heberle , J.J. Baumberg and K. Kohler, Appl. Phys Lett., **74**, 176 (2000)
[110] S. Chang, B. N. B. Rex, R.K. Chang, G. Chong and L.J. Guido, Appl. Phys. Lett., **75**, 166 (2000)
[111] S.X. Jin, J.Li, J.Z. Li, J.Y. Lin and H.X. Jiang, Appl. Phys. Lett., **76**, 631 (2000)
[112] R.A. Mair, K.C. Zeng, J.Y. Lin , H.X. Jiang, B. Zhang, L. Dai, A. Botchkarev, W. Kim, H. Morkoc, and M. A, Khan, Appl. Phys. Lett., **72**, 1530 (1998).
[113] R.P. Wang and MM. Dumitrescu, J. Appl. Phys., **81**, 3391 (1997)
[114] Powerful interface light emitting diodes for methane gas detection, A. Krier & V.V. Sherstnev, J. Phys. D: Appl. Phys. **33**, 101-106 (2000)